Cell Systems

Brief Report

Compression Generated by a 3D Supracellular Actomyosin Cortex Promotes Embryonic Stem Cell Colony Growth and Expression of Nanog and Oct4

Graphical Abstract

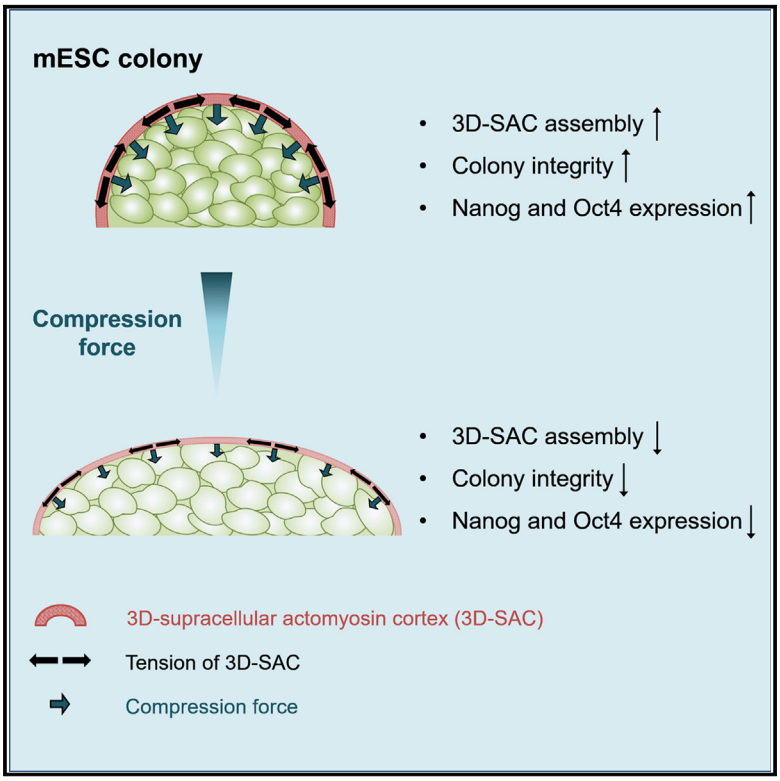

Highlights

- The surface tension of mESC colony is dynamically evolved during proliferation
- A 3D supracellular actomyosin cortex assembles around the colony surface of mESCs
- The compressive stress inside mESC colony facilitates pluripotency gene expression
- The 3D supracellular actomyosin cortex contributes to blastocyst development

Authors

Jing Du, Yanlei Fan, Zheng Guo, ..., Congying Wu, David A. Weitz, Xiqiao Feng

Correspondence

dringcin@126.com (J.D.), weitz@seas.harvard.edu (D.A.W.), fengxq@tsinghua.edu.cn (X.F.)

In Brief

Cells in an embryonic stem cell colony synergistically generate compression force by dynamically assembled cytoskeleton to facilitate the maintenance of colony morphology and pluripotency gene expression.

Du et al., 2019, Cell Systems 9, 214–220
July 24, 2019 © 2019 The Author(s). Published by Elsevier Inc.
https://doi.org/10.1016/j.cels.2019.05.008

CellPress

OPEN ACCESS
CellPress

Cell Systems
Brief Report

Compression Generated by a 3D Supracellular Actomyosin Cortex Promotes Embryonic Stem Cell Colony Growth and Expression of Nanog and Oct4

Jing Du,[1,2,4,10,11,*] Yanlei Fan,[1,10] Zheng Guo,[2,4] Youguang Wang,[1] Xu Zheng,[5] Chong Huang,[1] Baihui Liang,[6] Lingyu Gao,[7] Yanping Cao,[1] Yunping Chen,[1] Xi Zhang,[2,4] Lei Li,[8] Luping Xu,[6] Congying Wu,[9] David A. Weitz,[3,*] and Xiqiao Feng[1,*]
[1]Institute of Biomechanics and Medical Engineering, Department of Mechanical Engineering, School of Aerospace, Tsinghua University, Beijing 100084, China
[2]Key Laboratory for Biomechanics and Mechanobiology of Chinese Education Ministry, School of Biological Science and Medical Engineering, Beihang University, Beijing 100083, China
[3]Department of Physics and School of Engineering and Applied Sciences, Harvard University, Cambridge, MA 02138, USA
[4]Beijing Advanced Innovation Centre for Biomedical Engineering, Beihang University, Beijing 102402, China
[5]State Key Laboratory of Nonlinear Mechanics, Beijing Key Laboratory of Engineered Construction and Mechanobiology, Institute of Mechanics, Chinese Academy of Sciences, Beijing 100190, China
[6]Center for Nano and Micro Mechanics, School of Aerospace Engineering, Tsinghua University, Beijing 100084, China
[7]Department of Physics, Tsinghua University, Beijing 100084, China
[8]State Key Laboratory of Stem Cell and Reproductive Biology, Institute of Zoology, Chinese Academy of Sciences, Beijing 100101, China
[9]Institute of Systems Biomedicine, School of Basic Medical Sciences, Peking University Health Science Center, Beijing 100191, China
[10]These authors contributed equally
[11]Lead Contact
*Correspondence: dringcin@126.com (J.D.), weitz@seas.harvard.edu (D.A.W.), fengxq@tsinghua.edu.cn (X.F.)
https://doi.org/10.1016/j.cels.2019.05.008

SUMMARY

Mechanical factors play critical roles in mammalian development. Here, we report that colony-growing mouse embryonic stem cells (mESCs) generate significant tension on the colony surface through the contraction of a three-dimensional supracellular actomyosin cortex (3D-SAC). Disruption of the 3D-SAC, whose organization is dependent on the Rho/Rho-associated kinase (ROCK) signals and E-cadherin, results in mESC colony destruction. Reciprocally, compression force, which is generated by the 3D-SAC, promotes colony growth and expression of Nanog and Oct4 in mESCs and blastocyst development of mouse embryos. These findings suggest that autonomous cell forces regulate embryonic stem cells fate determination and provide insight regarding the biomechanical regulation of embryonic development.

INTRODUCTION

The mechanical microenvironment of cells, including stem cells, can regulate their physiology (Engler et al., 2006; Janmey and McCulloch, 2007; Shin et al., 2014). Embryonic stem cells (ESCs), which are derived from the inner cell mass (ICM) of embryos at the blastocyst stage, are mechanically sensitive and plastic. The variation range of the mechanical properties of ESCs is large (Young's modulus: 0.05 ~ 10 kPa), and the differentiation of ESCs is accompanied by significant alterations in the mechanical properties, including elasticity and viscosity (Kiss et al., 2011; Pillarisetti et al., 2011). Moreover, artificially applied mechanical stimuli, such as stretching, shear stress, and substrate stiffness, have profound effects on the fate determination of ESCs (Horiuchi et al., 2012; Lü et al., 2014; Wolfe and Ahsan, 2013). However, the biophysical mechanisms by which the intrinsic mechanical properties of ESCs are regulated have been rarely studied.

During embryonic development, groups of cells are organized as three-dimensional (3D) multilayer cell aggregates to cooperatively promote morphogenesis (Fleming, 1987; Maître et al., 2015). Similar to their organization within embryos, *in vitro* cultured ESCs are maintained and proliferate as 3D multilayer cell colonies, where cells adhere tightly to neighboring cells (Li et al., 2010). During differentiation, this 3D colony integrity is lost (Levenstein et al., 2006; Zhou et al., 2009), and inhibiting cell-cell adhesions or myosin contractility results in the loss of both colony structure and pluripotency (Li et al., 2010). Although the key roles of colony structure and integrity in ESCs fate determination have been noticed, the mechanisms by which the cell community autonomously generates force to maintain a 3D multilayer colony structure and further regulates pluripotency gene expression are still elusive. In this study, we observe the mechanical properties of mouse ESC (mESC) colonies during proliferation and differentiation and demonstrate that the contractile force generated by a 3D supracellular actomyosin cortex (3D-SAC) is required for mESC colony integrity. We also show that disruption of the 3D-SAC, whose organization is dependent on nonmuscle myosin II A (NMMIIA), Rho-ROCK signals, and E-cadherin, represses expression of the pluripotency genes, Nanog and Oct4.

 © 2019 The Author(s). Published by Elsevier Inc.
This is an open access article under the CC BY-NC-ND license (http://creativecommons.org/licenses/by-nc-nd/4.0/).

RESULTS

First, we performed single cell imaging analysis in cultured mESC colonies and found the cells in the outermost layer of the colony had an oblate shape, while those in the interior were nearly spherical (Figures S1A and S1D; Videos S1 and S2). The aspect ratios of the cells increased with increasing distances from the center of the colony (Figures S1B and S1E). In the outermost cells, the long axes of the oblate cells were approximately perpendicular to the radial direction of the colony (Figure S1C). This cellular morphology distribution indicated a strong circumferential stretch along the colony edge. To address whether there is significant tension on the colony surface, we focally ablated the edge of the colony by UV laser microscissors. Upon focal ablation, a distinct retraction was observed at the breakpoints, indicating a high tensile force on the colony surface (Figures 1A and 1B; Video S3). Next, we quantitatively measured the elastic modulus (E) on the colony surface by applying the indentation technique with atomic force microscopy (AFM). During colony growth, the Young's modulus (E) remained high ($\sim$200 Pa) before the growing colony reached a diameter of $\sim$80 μm, and then Young's modulus decreased dramatically with further proliferation (Figure 1C). Because the effective Young's modulus proportionally increased with the increasing magnitude of colony-surface tension shown by the theoretical analysis of the indentation technique (Mechanical Model in STAR Methods), these results suggest a significant mESC colony-surface tension, which dynamically evolves during cell proliferation.

The cytoskeleton has been proposed to be the primary contributor to the cell mechanics (Fletcher and Mullins, 2010). Thus, to determine the generation of the tension on the mESC colony surface, we analyzed the organizations of microtubules (MTs) and filamentous actin (F-actin). The results showed that while MTs were uniformly distributed among the cells throughout the colony, F-actin was enriched at the cell/medium boundary of the colony (Figures 1D and 1E). Because the contractility of F-actin is mediated by myosin motor proteins (Vicente-Manzanares et al., 2009), we further examined the organization of myosin and found that the NMMIIA network, but not NMMIIB, was substantially assembled at the cell/medium boundary and colocalized with F-actin bundles, forming a smooth and continuous actomyosin network (Figures S1F and S1G). This structure is similar to the "supracellular actomyosin ring" that is observed in wound healing and embryonic development (Brugués et al., 2014; Röper, 2013). However, as shown in Figure 1F and Videos S4, S5, and S6, the structure of the actomyosin network on the mESC colony surface is a 3D structure appearing as a cap that enclosed the colony that differs from the 2D "supracellular actomyosin ring". Thus, we named this distinctive architecture as "3D-supracellular actomyosin cortex (3D-SAC)". In addition, the 3D-SAC could also be observed in the Lifeact-mCherry and NMMIIA-mCherry expressing mESC colonies (Figures S1H and S1I).

During colony growth, the organization of 3D-SAC also showed a similar variation as the tension on colony surface (Figure 1C), with a peak at $\sim$72 h after seeding and a dramatic decrease thereafter. After leukemia inhibitory factor (LIF) withdrawal-induced differentiation, the 3D-SAC became nearly unobservable (Figures 1G and S1J). In addition, the 3D multilayer architecture was also impaired in large colonies, as evidenced by the decreased height/diameter ratio (Figures 1G and S1K). Notably, quantitative real-time PCR showed that the expression levels of Nanog, Oct4, and Esrrb (pluripotency markers) were also significantly decreased with increasing colony size, while the differentiation markers (Cdx2, Nestin, and Fgf5) were increased concurrently (Figures 1H and 1I).

To further examine the contribution of the 3D-SAC to the maintenance of mESCs functions, we locally disrupted it by UV laser microscissors. Disruption of 3D-SAC resulted in a rapid collapse of the colony within several minutes and finally led to loss of Nanog and Oct4 expression and reduced alkaline phosphatase (AP) staining intensity (Figures S2A–S2E). To specifically inhibit the contractility of the 3D-SAC without affecting myosin in other regions of the colony, we next used the photoactive myosin inhibitor Azidoblebbistatin (Ableb, also referred to as molecular tattoo) (Képiró et al., 2015) (Figure 1J). Immediately after Ableb tattooing, the 3D-SAC assembly was severely disrupted and the colonies became flattened within 1 h (Figures S2F–S2I). Furthermore, after continuous culture, the Nanog expression level and the AP staining intensity in the tattooed colonies were all significantly decreased compared with those in the control colonies (Figures 1K–1M). Thus, the integrity of the 3D-SAC assembly is crucial for sustaining the colony morphology and expression of Nanog and Oct4 genes in mESCs.

Next, we investigated the mechanism by which the 3D-SAC regulates colony integrity and Nanog and Oct4 expression. Considering the cap shape of the mESC colony and the continuity of cell-cell adhesions inside the colony, we proposed a mechanism analogous to the surface tension of a droplet cap dominated by the capillary effect. As shown in Figure 2A, the tension generated by the 3D-SAC resulted in an enhancement in the compressive pressure in the colony. We have measured and shown the existence and the effect of this tension by laser ablation and AFM (Figures 1A–1C). Besides, we employed particle image velocimetry (PIV) to demonstrate the significant mass flow in the colony after laser ablation (Figure 2B, the velocity field was calculated based on Video S3 and Figure 1A). The velocity distribution u(r) from the opening of the laser ablation approximately obeys $u(r) \sim 1/r^2$, where r is the distance to the opening (Figure S2J). This result is in line with the theoretical velocity field of a Stokes sink at the laser ablation opening, indicating the release of the internal compressive pressure (more details are provided in Section 2 of the Mechanical Model in STAR Methods). Similar results were also obtained by tracing the movement of fluorescence microbeads (FMBs) encapsulated inside the colony after laser ablation (Figure S2K; Videos S7). Overall, these results suggest that the contraction of the 3D-SAC increased the compressive stress in the interior of the colony.

Then, we speculated whether the compression force could promote the colony integrity and Nanog and Oct4 expression. First, we cultured mESC colonies in an immersion of low melting point (LMP) agarose gels with different concentrations (Figure 2C). During colony growth, the compression force generated by the agarose matrix on the colony increased with increasing agarose concentration, which was evidenced by the higher cell density and colony circularity in the denser agarose matrix (Figures S3A and S3B). To eliminate the effect of autonomous cell

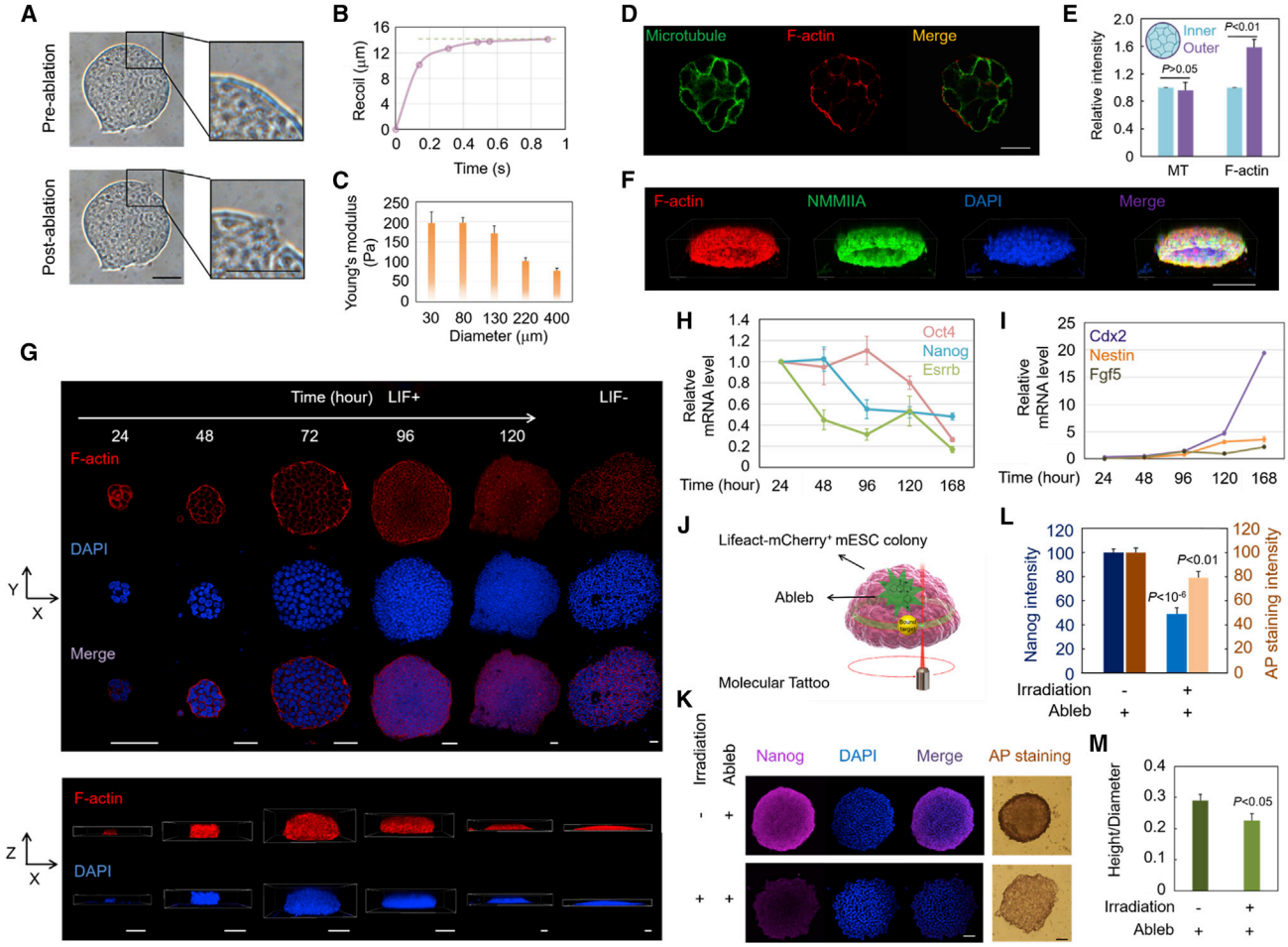

Figure 1. 3D-SAC Plays Crucial Roles in mESC Colony Integrity and Expression of Nanog and Oct4

(A) Representative images of laser ablation. The magnified views indicate the ablation location pre- and post-ablation. Scale bar: 30 μm.

(B) The recoil to time curve of laser ablation in (A).

(C) The variation trend of Young's modulus of mESC colony during colony growth measured by AFM (n = 13).

(D) XY slice images of microtubule immunostaining and Phalloidin staining of F -actin in R1 mESC colony. Scale bar: 15 μm.

(E) The statistical analysis of microtubule and F-actin intensity at cell-cell boundary (inner) and cell-medium boundary (outer) of colonies (n = 5).

(F) 3D reconstruction images of F-actin, NMMIIA, and nuclei in R1 mESC colony stained by Phalloidin, NMMIIA antibody, and DAPI, respectively. Scale bar: 20 μm.

(G) xy slice images of F-actin stained by Phalloidin in R1 mESC colonies growing for the indicated time after seeding in the presence of LIF (LIF+) or differentiated R1 mESC induced by LIF withdrawal (LIF−). Scale bar: 50 μm.

(H) Relative mRNA levels of Oct4, Nanog, and Esrrb during colony growth measured by quantitative real-time PCR (n = 3).

(I) Relative mRNA levels of Cdx2, Nestin, and Fgf5 during colony growth measured by quantitative real-time PCR (n = 3).

(J) The illustration of the molecular tattoo experiment using Ableb for specific inhibition of 3D-SAC in Lifeact-mCherry expressing R1 mESC colonies.

(K) xy slice images of Nanog immunostaining and AP staining 48 h after Ableb molecular tattoo experiment in tattooed colony (Irradiation+ and Ableb+) and control colony (Irradiation− and Ableb+). Scale bar: 50 μm.

(L) The statistical analysis of Nanog intensity (n = 10) and AP staining intensity (n = 8).

(M) The height to diameter ratios of R1 mESC colonies 48 h after the Ableb molecular tattoo experiment (n = 9). See also Figures S1 and S2 and Videos S1, S2, S3, S4, S5, and S6.

contraction of both interior cells and outer cells, the myosin inhibitor blebbistatin was added to the medium. As shown in Figure 2D, the cells treated with blebbistatin alone or in a low concentration agarose matrix (1%) showed a more substantial loss of Oct4-GFP expression, while cells in the denser agarose matrix (2% and 5%) showed remarkable increasing expression of Oct4-GFP and improved colony integrity (Figures 2D, 2E, and S3C). In addition, we also applied a compression force to mESC colonies by culturing the cells in microfabricated PDMS (polydimethylsiloxane) microwells (Figures S3D and S3E). After LIF withdrawal-induced differentiation, cells growing on a 2D planar substrate (2D culture) were substantially differentiated, while cells growing inside the microwells retained a high level of Oct4-GFP expression (Figures S3F–S3H). These results

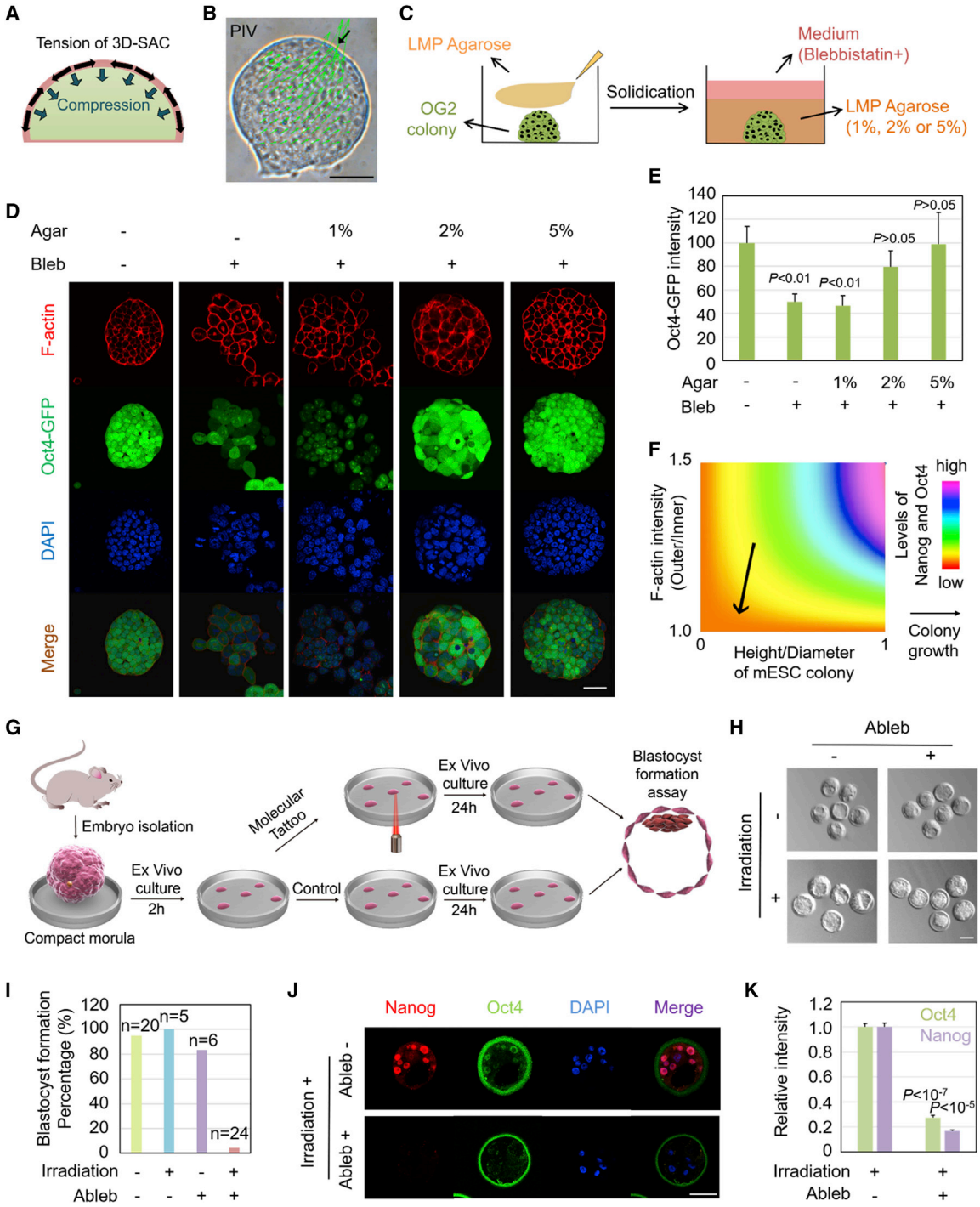

Figure 2. 3D-SAC Contractility Enhances the Compressive Stress to Facilitate Nanog and Oct4 Expression and Blastocyst Development

(A) Schematic illustration of compressive force on mESC colony surface generated by the tension of 3D-SAC.

(B) The PIV velocity field in the mESC colony, calculated based on the motion of cells in the colony in 2 s after laser ablation. The green arrows are the velocity vectors, and the black arrow indicates the opening of the laser ablation. Scale bar: 30 μm.

(C) Experimental strategy for agarose constraint applied to OG2 mESC colonies.

(D) Fluorescent staining images of F-actin and Oct4-GFP in OG2 colonies cultured in LMP agarose with different concentrations in the presence of blebbistatin (Bleb +, 25 μM). Scale bar: 50 μm.

(E) The statistical analysis of Oct4-GFP intensity (n = 10).

(F) The numerical simulation model of the correlation between 3D-SAC construction (O/I ratio of F-actin intensity), the 3D construction of colony (height/diameter ratio), and the expression of Nanog and Oct4. The variation trend during colony growth was also indicated by the arrow.

(legend continued on next page)

suggest that compression force could effectively promote the colony maintenance and Oct4-GFP expression of mESCs. Based on the above-mentioned experiments, we proposed a biomechanical model to calculate the interior pressure in the colony and developed a framework describing the relationships of 3D-SAC assembly, colony organization, and Nanog and Oct4 expression during cell proliferation (Figure 2F and Mechanical Model in STAR Methods).

Next, to identify the mechanism by which the 3D-SAC is organized, we investigated the distributions of NMMIIA in the colony. At the 2-cell stage, the actomyosin network was distributed over the entire cell-medium boundary, with a significant enrichment at the apical-lateral border along the cell-cell junctions (Figure S4A), indicating the potential contribution of intercellular connections. Then, we assessed the major intercellular adhesion molecules. As shown in Figures S4B and S4C, adherens junction (AJ) proteins (E-cadherin and α-catenin) were observed enriched at the apical-lateral borders along the cell-cell junctions and colocalized with NMMIIA, while the tight junction component ZO-1 and gap junction protein connexin 43 did not show distinct colocalization with NMMIIA. These findings were also confirmed in larger colonies (Figure S4C). Furthermore, E-cadherin siRNA substantially disrupted 3D-SAC organization and the 3D structure of mESC colonies, while siRNA interference of ZO-1 and connexin 43 did not show a significant effect (Figures S5A–S5D). Moreover, E-cadherin siRNA treatment or specifically inhibition of the E-cadherin in the outer cells by E-cadherin neutralization antibody resulted in a significant decrease in the Oct4 expression in mESCs (Figures S5E–S5H).

The activity of myosin II is mainly regulated by the phosphorylation of its light chain (MLC) through myosin light chain kinase (MLCK) and ROCK (Amano et al., 1996; Ikebe and Hartshorne, 1985). In our experiments, we found that phospho-MLC2 was also enriched at the cell-medium boundary of the colonies (Figures S6A and S6B) and inhibition of ROCK by its inhibitor Y27632 substantially abrogated the assembly of the 3D-SAC and Nanog expression, while the MLCK inhibitor ML-7 showed a subtle effect (Figures S6C–S6E). ROCK is a downstream effector of the Rho subfamily of small GTPases (Matsui et al., 1996). Using a FRET biosensor (Yoshizaki et al., 2003), we found drastic activation of RhoA at the cell-medium boundary compared with that along the cell-cell boundary throughout the colony (Figures S6F and S6G). Overexpression of a constitutively activated RhoA significantly enhanced the 3D-SAC assembly and Oct4 expression (Figures S7A–S7C) without affecting cell proliferation (Figures S7D and S7E). To specifically inhibit the Rho/ROCK signaling in the outer cells, we used a Rho inhibitor (Rho inhibitor I, CT04, Cytoskeleton) with a covalently linked cell-penetrating moiety, which will be released once in the cytosol. Thus, the inhibitor could not permeate furtherly into the interior of the colony and only inhibited the activity of Rho signaling in the outer cells. The results showed that the inhibition of the Rho signaling in the outer cells significantly affected the organization of the 3D-SAC (Figures S7F and S7G).

Recently, Maître et al. reported that pulsatile contractility generated by an actomyosin cortex plays an important role in the compaction of mouse embryos at the 8-cell stage (Maître et al., 2015). Since mESCs are originally derived from the ICM of mouse blastocysts, we then assessed the function of the compression force generated by the actomyosin cortex in the further embryonic development and expression of Nanog and Oct4. First, we measured the mechanical characteristics of early embryos by AFM, and the results indicated a significant increase in Young's modulus at the 8-cell stage after compaction (Figure S8A). Moreover, the 3D-SAC was formed after 8-cell compaction that occurred until the stage of blastocyst during pre-implantation development (Figures S8B–S8D). Moreover, disruption of the 3D-SAC by molecular tattoo in the morula caused a substantial failure of further development to blastocyst (the success rate was less than 5%; Figures 2G–2I), and the expression levels of Nanog and Oct4 were also significantly decreased in the tattooed embryos compared with the control embryos (Figures 2J, 2K, S8E, and S8F). These results indicate that the contractility of 3D-SAC is essential in the blastocyst development and expression of Nanog and Oct4 in mouse embryos.

DISCUSSION

In this work, we revealed a vital function of compression force generated by a 3D supracellular cytoskeleton network in regulating the architecture and expression of Nanog and Oct4 both in cultured ESCs and embryos. Our results also particularly highlight the functions of the mechanical microenvironment in the colony construction and expression of Nanog and Oct4 in ESCs. Therefore, the coupled biological, chemical, and mechanical relationship between cells and the extracellular microenvironment collectively determines cell fate and has potential applications in the understanding of embryonic development.

STAR★METHODS

Detailed methods are provided in the online version of this paper and include the following:

- KEY RESOURCES TABLE
- CONTACT FOR REAGENT AND RESOURCE SHARING
- EXPERIMENTAL MODEL AND SUBJECT DETAILS
  - Cell Lines
  - Animal Model

(G) The experimental strategies for investigating the role of 3D-SAC in early mouse embryo development using molecular tattoo technique.
(H) Images of embryo morphology in molecular tattoo group (Irradiation+ and Ableb+) and control groups (Irradiation− and Ableb−; Irradiation−, and Ableb+; and Irradiation+ and Ableb−). Scale bar: 50 μm.
(I) The statistical analysis of blastocyst formation efficiency in molecular tattoo (Irradiation+, Ableb+) and control groups (Irradiation-, Ableb-; Irradiation-, Ableb+; Irradiation+, Ableb-).
(J) Immunostaining images of pluripotent genes (Nanog and Oct4) in embryos of molecular tattoo group (Irradiation+ and Ableb+) and control group (Irradiation+ and Ableb−). Scale bar: 50 μm.
(K) The statistical analysis of Nanog and Oct4 expression levels in molecular tattooed embryos and control embryos (n = 5). See also Figures S3–S8 and Video S7.

- METHOD DETAILS
  - AFM Experiment
  - Immunofluorescence
  - Plasmid, siRNA and Transfection
  - Real-Time qPCR
  - FRET Measurements
  - AP Assay
  - Cell Proliferation Analysis
  - Molecular Tattoo
  - Laser Microscissors
  - PIV (Particle Image Velocimetry) Measurement
  - Mouse Embryo Experiment
  - Agarose Restraint Assay
  - Micro-well PDMS Pad Preparation and Cell Culture
- QUANTIFICATION AND STATISTICAL ANALYSIS
  - Mechanical Model

SUPPLEMENTAL INFORMATION

Supplemental Information can be found online at https://doi.org/10.1016/j.cels.2019.05.008.

ACKNOWLEDGMENTS

We thank Y.G. Chen (Tsinghua University) and D.Q. Pei (Chinese Academy of Sciences) for providing R1 and OG2 cell lines, respectively. We also thank M. Long (Chinese Academy of Sciences), Y. Liang (EV-bio), X.H. Shi (Chinese Academy of Sciences), X. Liang (Tsinghua University), H.W. Wang (Tsinghua University), G.S. Ou (Tsinghua University), Z.C. Chen (Tsinghua University), S.J. Huang (Tsinghua University), and B. Li (Tsinghua University) for technical assistance and discussions during the preparation of this paper. This work was supported by the National Key R&D Program of China (2017YFA0506500), the National Natural Science Foundation of China (31370018 and 11620101001) and Fundamental Research Funds for the Central Universities (ZG140S1971). D.A.W. was supported in part by the NSF (DMR-1708729) and the Harvard MRSEC (DMR-1420570).

AUTHOR CONTRIBUTIONS

J.D., Y.F., X.F., and D.A.W. designed the study and performed and interpreted experiments. Y.W., C.H., and Yanping Cao helped with AFM experiments. Z.G. and C.H. performed the mouse embryo experiments. Yunping Chen helped with mouse embryonic stem cell culture. B.L. and L.X. performed the microwell experiments. Xu Zheng performed the PIV analysis. J.D., Xi Zhang, Xu Zheng, L.G., X.F., and Yanping Cao carried out the theoretical analysis and data analysis. L.L. and C.W offered technical support in mouse embryo experiments and cytoskeleton analysis, respectively. J.D., D.A.W., and X.F. conceived and supervised this project and prepared the paper.

DECLARATION OF INTERESTS

The authors declare no competing interests.

Received: March 9, 2018
Revised: December 19, 2018
Accepted: May 22, 2019
Published: July 3, 2019

REFERENCES

Amano, M., Ito, M., Kimura, K., Fukata, Y., Chihara, K., Nakano, T., Matsuura, Y., and Kaibuchi, K. (1996). Phosphorylation and activation of myosin by Rho-associated kinase (Rho-kinase). J. Biol. Chem. *271*, 20246–20249.

Brugués, A., Anon, E., Conte, V., Veldhuis, J.H., Gupta, M., Colombelli, J., Muñoz, J.J., Brodland, G.W., Ladoux, B., and Trepat, X. (2014). Forces driving epithelial wound healing. Nat. Phys. *10*, 683–690.

Ding, Y., Niu, X.R., Wang, G.F., Feng, X.Q., and Yu, S.W. (2016). Surface effects on nanoindentation of soft solids by different indenters. Mater. Res. Express *3*, 11.

Engler, A.J., Sen, S., Sweeney, H.L., and Discher, D.E. (2006). Matrix elasticity directs stem cell lineage specification. Cell *126*, 677–689.

Fleming, T.P. (1987). A quantitative analysis of cell allocation to trophectoderm and inner cell mass in the mouse blastocyst. Dev. Biol. *119*, 520–531.

Fletcher, D.A., and Mullins, R.D. (2010). Cell mechanics and the cytoskeleton. Nature *463*, 485–492.

Horiuchi, R., Akimoto, T., Hong, Z., and Ushida, T. (2012). Cyclic mechanical strain maintains Nanog expression through PI3K/Akt signaling in mouse embryonic stem cells. Exp. Cell Res. *318*, 1726–1732.

Huveneers, S., and de Rooij, J. (2013). Mechanosensitive systems at the cadherin–F-actin interface. J. Cell Sci. *126*, 403–413.

Ikebe, M., and Hartshorne, D.J. (1985). Phosphorylation of smooth muscle myosin at two distinct sites by myosin light chain kinase. J. Biol. Chem. *260*, 10027–10031.

Jacobelli, J., Bennett, F.C., Pandurangi, P., Tooley, A.J., and Krummel, M.F. (2009). Myosin-IIA and ICAM-1 regulate the interchange between two distinct modes of T cell migration. J. Immunol. *182*, 2041–2050.

Janmey, P.A., and McCulloch, C.A. (2007). Cell mechanics: integrating cell responses to mechanical stimuli. Annu. Rev. Biomed. Eng. *9*, 1–34.

Képiró, M., Várkuti, B.H., Rauscher, A.A., Kellermayer, M.S.Z., Varga, M., and Málnási-Csizmadia, A. (2015). Molecular tattoo: subcellular confinement of drug effects. Chem. Biol. *22*, 548–558.

Kiss, R., Bock, H., Pells, S., Canetta, E., Adya, A.K., Moore, A.J., De Sousa, P., and Willoughby, N.A. (2011). Elasticity of human embryonic stem cells as determined by atomic force microscopy. J. Biomech. Eng. *133*, 101009.

Levenstein, M.E., Ludwig, T.E., Xu, R.H., Llanas, R.A., VanDenHeuvel-Kramer, K., Manning, D., and Thomson, J.A. (2006). Basic fibroblast growth factor support of human embryonic stem cell self-renewal. Stem cells *24*, 568–574.

Li, D., Zhou, J., Wang, L., Shin, M.E., Su, P., Lei, X., Kuang, H., Guo, W., Yang, H., Cheng, L., et al. (2010). Integrated biochemical and mechanical signals regulate multifaceted human embryonic stem cell functions. J. Cell Biol. *191*, 631–644.

Li, Z., Fei, T., Zhang, J., Zhu, G., Wang, L., Lu, D., Chi, X., Teng, Y., Hou, N., Yang, X., et al. (2012). BMP4 Signaling Acts via dual-specificity phosphatase 9 to control ERK activity in mouse embryonic stem cells. Cell Stem Cell *10*, 171–182.

Lü, D., Luo, C., Zhang, C., Li, Z., and Long, M. (2014). Differential regulation of morphology and stemness of mouse embryonic stem cells by substrate stiffness and topography. Biomaterials *35*, 3945–3955.

Maître, J.L., Niwayama, R., Turlier, H., Nédélec, F., and Hiiragi, T. (2015). Pulsatile cell-autonomous contractility drives compaction in the mouse embryo. Nat. Cell Biol. *17*, 849–855.

Matsui, T., Amano, M., Yamamoto, T., Chihara, K., Nakafuku, M., Ito, M., Nakano, T., Okawa, K., Iwamatsu, A., and Kaibuchi, K. (1996). Rho-associated kinase, a novel serine/threonine kinase, as a putative target for small GTP binding protein Rho. EMBO J. *15*, 2208–2216.

Pillarisetti, A., Desai, J.P., Ladjal, H., Schiffmacher, A., Ferreira, A., and Keefer, C.L. (2011). Mechanical phenotyping of mouse embryonic stem cells: increase in stiffness with differentiation. Cell. Reprogram. *13*, 371–380.

Röper, K. (2013). Supracellular actomyosin assemblies during development. BioArchitecture *3*, 45–49.

Shin, J.W., Buxboim, A., Spinler, K.R., Swift, J., Christian, D.A., Hunter, C.A., Léon, C., Gachet, C., Dingal, P.C., Ivanovska, I.L., et al. (2014). Contractile forces sustain and polarize hematopoiesis from stem and progenitor cells. Cell Stem Cell *14*, 81–93.

Shrestha, D., Jenei, A., Nagy, P., Vereb, G., and Szollosi, J. (2015). Understanding FRET as a research tool for cellular studies. Int. J. Mol. Sci. *16*, 6718–6756.

Smyth, J.W., Vogan, J.M., Buch, P.J., Zhang, S.S., Fong, T.S., Hong, T.T., and Shaw, R.M. (2012). Actin cytoskeleton rest stops regulate anterograde traffic of connexin 43 vesicles to the plasma membrane. Circ. Res. *110*, 978–989.

Thielicke, W., and Stamhuis, E.J. (2014). PIVlab – Towards user-friendly, affordable and accurate digital particle image velocimetry in MATLAB. J. Open Res. Software *2*, e30.

Vicente-Manzanares, M., Ma, X., Adelstein, R.S., and Horwitz, A.R. (2009). Non-muscle myosin II takes centre stage in cell adhesion and migration. Nat. Rev. Mol. Cell Biol. *10*, 778–790.

Wolfe, R.P., and Ahsan, T. (2013). Shear stress during early embryonic stem cell differentiation promotes hematopoietic and endothelial phenotypes. Biotechnol. Bioeng. *110*, 1231–1242.

Yoshizaki, H., Ohba, Y., Kurokawa, K., Itoh, R.E., Nakamura, T., Mochizuki, N., Nagashima, K., and Matsuda, M. (2003). Activity of Rho-family GTPases during cell division as visualized with FRET-based probes. J. Cell Biol. *162*, 223–232.

Zhou, J., Su, P., Wang, L., Chen, J., Zimmermann, M., Genbacev, O., Afonja, O., Horne, M.C., Tanaka, T., Duan, E., et al. (2009). mTOR supports long-term self-renewal and suppresses mesoderm and endoderm activities of human embryonic stem cells. Proc. Natl. Acad Sci. USA *106*, 7840–7845.

STAR★METHODS

KEY RESOURCES TABLE

REAGENT or RESOURCE	SOURCE	IDENTIFIER
Antibodies		
Rabbit monoclonal anti-Tubulin	Abcam	Cat# ab6046; RRID: AB_2210370
Mouse monoclonal anti-NMMIIA (clone DM1A)	Abcam	Cat# ab24762; RRID: AB_2282292
Rabbit polyclonal anti-NMMIIB	Abcam	Cat# ab684; RRID: AB_305661
Rabbit polyclonal anti-Nanog	Abcam	Cat# ab80892; RRID: AB_2150114
Rabbit polyclonal anti-Oct4	Abcam	Cat# ab19857; RRID: AB_445175
Rabbit polyclonal anti-E-cadherin	Abcam	Cat# ab11512; RRID: AB_298118
Rabbit polyclonal anti-alpha-catenin	Abcam	Cat# ab51032; RRID: AB_868700
Rabbit polyclonal anti-ZO1	Abcam	Cat# ab59720; RRID: AB_946249
Rabbit polyclonal anti-Connexin43	Abcam	Cat# ab11370; RRID: AB_297976
Rabbit polyclonal anti-phospho-MLC2	Cell signaling	Cat# 3671; RRID: AB_330248
Rabbit polyclonal anti-E-cadherin (DECMA-1)	Biolegend	Cat# 147301; RRID: AB_2563037
Chemicals, Peptides, and Recombinant Proteins		
ML-7	Sigma-Aldrich	I2764
Y-27632	Sigma-Aldrich	Y0503
azidoblebbistain (ABleb)	Optopharma	DR-A-081
Rho Inhibitor I	Cytoskeleton, Inc.	CT04
CHIR99021	Sigma-Aldrich	SML1046
PD0325901	Sigma-Aldrich	PZ0162
Alexa Flour 488 phalloidin	Invitrogen	A12379
Alexa Flour 568 phalloidin	Invitrogen	A12380
Alexa Flour 647 phalloidin	Invitrogen	A22287
Blebbistatin	Sigma-Aldrich	B0560
Critical Commercial Assays		
FastQuant RT Kit	TIANGEN	KR106
KOD-Plus-Mutagenesis Kit	TOYOBO	SMK-101
BCIP/NBT Alkaline Phosphatase Color Development Kit	Beyotime Institute of Biotechnology	P0321
keyFluor488 Click-iT EdU imaging detection kit	KeyGEN BioTECH	KGA331
Experimental Models: Cell Lines		
R1 Mouse embryonic stem cells	Yeguang Chen, (Tsinghua University (Li et al., 2012))	RRID:CVCL_2167
OG2 Mouse embryonic stem cells	Duanqing Pei (Chinese Academy of Sciences)	N/A
Primary mouse embryonic fibroblasts	This study	N/A
Experimental Models: Organisms/Strains		
CD-1 (ICR) IGS Mice	Beijing Vital River Laboratory Animal Technology	Stock No.: 201
Oligonucleotides		
siRNA targeting sequence: see Table SI	This paper	N/A
Primers for Real-time PCR, see Table S2	This paper	N/A
Recombinant DNA		
EYFP-membrane	Clontech Laboratories	6917–1
pDEST-Lifeact-mCherry	(Smyth et al., 2012)	RRID:Addgene_40908
pEF1/Myc-His B	Invitrogen	V921-20
pEF1/Myc-His B-Lifeact-mCherry	This paper	N/A
myosin-IIA-GFP	(Jacobelli et al., 2009)	RRID:Addgene_38297

(*Continued on next page*)

Continued

REAGENT or RESOURCE	SOURCE	IDENTIFIER
pEF1/Myc-His B-myosin IIA-mCherry	This paper	N/A
RaichuEV-RhoA/KRasCT	Professor Michiyuki Matsuda (Kyoto University)	10319
pRK5-myc-RhoA-Q63L	http://n2t.net/addgene:12964	RRID:Addgene_12964
Software and Algorithms		
PIVLab v1.41	Thielicke and Stamhuis (2014)	N/A
ImageJ	https://imagej.net/	RRID:SCR_003070
MATLAB	The MathWorks	RRID:SCR_001622

CONTACT FOR REAGENT AND RESOURCE SHARING

Further information and requests for resources and reagents should be directed to and will be fulfilled by the Lead Contact, Jing Du (dringcin@126.com)

EXPERIMENTAL MODEL AND SUBJECT DETAILS

Cell Lines

Mouse embryonic stem cells (R1 and OG2) were routinely cultured on the feeders covered or feeder-free for different experimental purposes. The medium was DMEM supplemented with 4.5 g/L glucose and L-glutamine (Corning), 15% knockout serum replacement (Invitrogen), 100 μM 2-mercaptoethanol (Sigma), 1×penicilin-streptomycin (Corning), 1 mM non-essential amino acids (Corning) and 1000 U/ml LIF (Millipore) in the feeder covered culture. In the feeder-free culture medium, serum was replaced with Fetal Bovine Serum Defined (HyClone) and CHIR99021 and PD0325901 were added with a work concentration of 3 μM and 1 μM, respectively. Petri dishes were coated with 0.1% gelatin (Millipore) for 30 min at room temperature before seeding cells. Cells were grown at 37 °C in an incubator with 5% CO_2. The mouse ES cell lines were authenticated by their typical morphology and functional assays.

Animal Model

All mice were bred and housed at Tsinghua University Animal Facilities under a 12-hour light/dark cycle (light period 7:00–19:00) at 22°C. Food and water were available ad libitum. All of the experimental procedures were performed with the approval of the Institutional Animal Care and Use Committee (IACUC) of Tsinghua University. Tsinghua University Animal Facilities has been accredited by the Association for Assessment and Accreditation of Laboratory Animal Care International (AAALAC).

METHOD DETAILS

AFM Experiment

The AFM (NT-MDT) equipped with an optical microscope system (IX71, Olympus) was used to estimate the equivalent stiffness of embryonic stem cells. Indentation was done with a silicon nitride cantilever with a spherical polystyrene tip. The cantilever used for these experiments was 200 μm long, 15 μm wide, and 550 nm thick, with a spring constant is 0.05 N/m (MLCT-O10). The radius of tip used here was 5 μm. For each cell colony, 9 positions were selected in the scale of 30 μm × 30 μm for the indentation experiment. The curves were fitted with the Hertz model:

$$F = \frac{4ER^{0.5}}{3(1-\nu^2)}\delta^{1.5}$$

in which, E is the elastic modulus of the cell. ν is the Poisson's ratio of the cell material and ν = 0.5 in general. R is the radius of the ball head on the cantilever beam. δ is the deformation distance of the cell and F is the force between the probe and cell colony.

The average value of those nine measurements was defined as the cell stiffness with the loading rate of 5 μm/s and the loading depth of 400 nm. Experiments were replicated at least three times.

Immunofluorescence

Cells grown on glass bottom dishes were washed 3 times with pre-warmed PBS before fixed with 4% PFA for 30 min at room temperature. Cells were permeabilized with 0.2% Triton X-100 for 10 min and fixed with 4% PFA for 5 min at RT again. After 3 times washed with 0.1% PBST, cells were blocked with 5% BSA (Sigma) solution in PBS for 2 hr at RT. Cells were incubated with primary antibodies (Abcam) at the optimal concentrations (according to the manufacturer's instructions) at 4 °C overnight. After washing, cells were incubated for 2 hr with secondary antibodies: 488/568/633 IgG (H+L) and/or Alexa Flour 488/568/647 phalloidin (Invitrogen) for 40 min. Nuclei were stained with DAPI (4',6-diamidino-2-phenylindole, Invitrogen) for 10 min at RT. Confocal images were taken on the Nikon A1R microscope equipped with a 60× objective. Experiments were replicated at least three times.

Plasmid, siRNA and Transfection

Lifeact-mCherry gene was amplified from a pDEST vector (Addgene) using the primers with a Kozak sequence, forward, CGGAATTCGCCACCATGGGCGTGGCCGACCTGAT, reverse, TAAAGCGGCCGCTTACTTGTACAGCTCG. The purified PCR products and pEF1/Myc-His B (Invitrogen) were dissected by restriction enzymes, Kpn I and Not I, and the recombinant plasmid of pEF1/Myc-His B-Lifeact-mCherry was constructed *in vitro*.

Myosin IIA was amplified from myosin-IIA-EGFP (Addgene) using the following primers, forward, GGGGTACCATGGCTCAGCA GGCTGCAGAC, reverse, TCCCGGATATCTCGATTCAGCTGCCTTGGCATCGG. The purified PCR products and pEF1/Myc-His B-Lifeact-mCherry were dissected by restriction enzymes, Kpn I and EcoR V, and then the recombinant plasmid of pEF1/Myc-His B-myosin IIA-mCherry was constructed. Fugene HD (Promega) was used for plasmid-DNA transfections according to the manufacturer's instructions. The stable expression cell strains were selected using Geneticin (Invitrogen) with 500 μg/ml.

For genes silence assay, duplex siRNA sequences were designed for the downregulation of ZO-1, Connexin 43, Arp 2 and E-cadherin (Table S1). R1 cells were pre-plated on the 60 mm petri dishes for 48 hr. Lipofectamine RNAiMAX Reagent (Invitrogen) was used for siRNA transfection, after that cells were continued to cultivate for 48 hr.

Real-Time qPCR

Total RNA was extracted from cells on petri dishes using Trizol (Invitrogen) following the manufacturer's instructions. Complementary DNA was synthesized with oligo-dT primer using the FastQuant RT Kit (TIANGEN). The expression level of target genes were detected by using Mastercycler ep realplex (Eppendorf) in 20 μL reaction volumes containing 10 μL of SYBR Green PreMix (TIANGEN), 0.3 μM of each primer and 20× diluted cDNA. Thermal cycling conditions were followed the manufacturer's protocol. Primer sequences were listed in Table S2. Before formal experiment, all primer pairs were checked by melt-curve analysis. GAPDH was chosen as internal reference for the calibrator of relative mRNA levels. Experiments were replicated at least three times.

FRET Measurements

RhoA FRET probe plasmid (pPBbsr-Raichu-2707x) was a gift from Professor M. Matsuda (Osaka University, Osaka, Japan). FRET efficiency was measured in living cells by the three-channel emission method in a confocal laser scanning microscope (A1RMPSi, Nikon). For three-channel emission measurement, the donor alone, acceptor alone plasmids were reconstructed from pPBbsr-Raichu-2707x through deleting mutant with KOD-Plus-Mutagenesis Kit (TOYOBO). The signals were collected from donor alone, acceptor alone and doubly (donor-and-acceptor) labeled cells respectively under the same laser scanning parameters. Then, corrected FRET (F^c) method was used for fluorescence from background and bleed-through with the following form:

$F^c = F_f - [(F_d/D_d)\times D_f] - [(F_a/A_a) \times A_f]$ (Shrestha et al., 2015)

In the above equation, F_f, D_f and A_f represent the FRET, Donor and Acceptor channels of the FRET sample, F_d, and D_d represent the FRET and Donor channels of the donor samples, F_a and A_a represent the FRET and Acceptor channels of the acceptor sample, respectively. FRET efficiency (F^e) was calculated by the following following formula:

$F^e = (F^c / D_f)\times 100$. Experiments were replicated at least three times.

AP Assay

Alkaline phosphatase (AP) staining was performed with BCIP/NBT Alkaline Phosphatase Color Development Kit (Beyotime Institute of Biotechnology) according to the manufacturer's protocol. Briefly, cells were fixed with 4% PFA for 15 min at room temperature, washed with PBS and then incubated with BCIP/NBT solution for 25 min, operation in the dark room. Finally, the cells were photographed using optical microscope (Olympus, IX71) equipped with a 40× objective. Experiments were replicated at least three times.

Cell Proliferation Analysis

The mESCs were cultured on confocal plates for 4 days, and then incubated with 10 μM 5-ethynyl-2'-deoxyuridine (EdU; KeyGEN BioTECH, China) for 30 min before fixed with 4% PFA. EdU detection was strictly performed following manufacturer's instructions of keyFluor488 Click-iT EdU imaging detection kit (KeyGEN BioTECH, China). Experiments were replicated at least three times.

Molecular Tattoo

A photoreactive myosin II-specific inhibitor, azidoblebbistain (ABleb) was dissovled in DMSO with a 3 mM stock concentration, protected from light. Cells were incubated with FBS-free DMEM containing 6 μM ABleb for 30 min at 37 °C before bleaching. The edge of colonies were chosen as target for bleaching with a reverse Two-Photon Microscope (A1RMPSi, Nikon) equipped with a live cell station. Cells were raster scanned for 10 s with 860 nm (λ_{ex}) light wave at 35% laser power, using a 60× water objective. Experiments were replicated at least three times.

Laser Microscissors

Microscissors experiments were performed on a fluorescence microscope (LMD7000, Leica) equipped with a 37 °C heating stage, using a 60× dry objective. Optimized cutting parameters as following were used for ablating F-actin, laser power: 59%, aperture: F22, speed: 4 ms, Pulse Frequency: 1046 Hz. Time-lapse images were acquired with an interval of 40 ms per frame after ablation. Cells were fixed with 4% PFA after ablation immediately or cultured for 48 hr and then fixed, respectively. Experiments were replicated at least three times.

PIV (Particle Image Velocimetry) Measurement

PIV is a method of flow visualization that provides the velocity field based on correlation calculation of the digital images. We used two images from Video S3 to calculate the displacements of the cells in the colony. The first image was captured just after the laser ablation, and the second one was $\Delta t = 2$ sec after that. As the motions of the cells inside the colony due to the release of the compressive pressure were clearly observed in the images, we did not need to add tracers to visualize this mass flow. The correlation algorithm was coded using Matlab in our lab. An interrogation area of 128 × 64 pixels was chosen during correlation calculation to search the correlation peaks. The distance of the correlation peaks represented the displacement of the corresponding cells in 2 sec. Therefore, the velocity field (as shown by the green vectors in Figure 2B) was calculated as $\mathbf{u} = \mathbf{L}/\Delta t$, where $\mathbf{L}$ was the displacement vector. Experiments were replicated at least three times.

Mouse Embryo Experiment

Embryos were isolated from superovulated female ICR mice mated with male mice. Superovulation of female mice is induced by intraperitoneal injection of 10 international units (IU) of pregnant mare's serum gonadotropin (PMSG), followed by intraperitoneal injection of 10 IU human chorionic gon adotropin (hCG) 44–48 hr later. Morula-stage (E2.5) embryos were recovered by flushing uterus from plugged females with 37 °C M2 medium (Sigma) using an injection syringe (zymm HX-Z08). Embryos were handled using an aspirator tube equipped with a glass pipette pulled from glass micropipettes. Embryos were placed in KSOM+AA (caisson, IVL04) in 20-μl droplets covered in mineral oil (Sigma). Embryos were cultured in an incubator with a humidified atmosphere supplemented with 5% CO_2 at 37 °C. Experiments were replicated at least three times.

Agarose Restraint Assay

Low-melting-agarose (LMA) was confected into PBS solution with 1%, 2% and 5% different concentrations respectively. These complexes were sterilized by autoclaving, after that cooled down to 42 °C on a heating block which cloud maintain a stability temperature to keep these complexes in a liquid stage. OG2 cells were cultured with normal medium for 72 hr in confocal plates until they formed clone morphology, then removed the medium and pipe the prepared different concentrated agarose into the plates. Cool down to room temperature till LMA become concretionary. Next, cells were cultured for 48 hr with normal or containing 25 μM blebbistain mediums. Experiments were replicated at least three times.

Micro-well PDMS Pad Preparation and Cell Culture

A silicon wafer was spin-coated with resist SU8-2050 (MicroChem). Predesigned features were patterned on a mask through an electron-beam lithography system. Then UV exposure was applied for 10 sec to make sure the exposure energy between 150 mJ/cm^2 -215 mJ/cm^2. The exposed resist was removed by Micro-Chem's SU8 developer. When using SU-8 developer, spray and wash the developed image with fresh solution for approximately 10 sec, followed by a second spray/wash with Isopropyl Alcohol (IPA) for another 10 sec. After air dried with filtered, pressurized air or nitrogen, the master was ready. We prepared PDMS micro-well by replica molding the master. PDMS (A:B = 10:1) was poured on the masters and allowed to gel for about 1.5 hr at 80 °C. The slab of PDMS was peeled away from the master, and then 0.1% gelatin was coated on the pad for 30 min at room temperature. Then OG2 cells were placed on the PDMS substrate and cultured at 37 °C in an incubator for overnight. Experiments were replicated at least three times.

QUANTIFICATION AND STATISTICAL ANALYSIS

The number of biological replicates in each experimental result was indicated in the figure legends. Data were presented as means ± SEM. Significance was determined using Student's t test to compare the differences between two experimental groups.

Mechanical Model

To explain the causation of the 3D-SAC, we develop a theoretical model. The stress boundary conditions of the colony read:

$$\sigma_{ij} l_i = T_j$$

where σ is the stress tensor in the colony, l is the unit vector normal to the colony surface, and T is the surface traction vector.

The stress has a high concentration at the cell-cell junctions on the colony surface (Figure S3J). The cells respond to the mechanical signal by F-actin remodeling to the stress in the colony (Huveneers, and de Rooij, 2013). Meanwhile, the stress in the colony is nearly uniform or, in other words, $\nabla \boldsymbol{\sigma} \approx 0$. As a result, the intensity of F-actin at the colony surface was observed to be significantly higher than that inside the colony. The surface stress was further increased with the promoted assembly of F-actin, which continued to increase because of the positive feedback until the biochemical limit.

The tension of the 3D-SAC induces a higher interior compressive stress in the colony (Figure 2A). On the basis of our experimental data, we calculate the surface tension in the colony, which is regarded as an elastomer body covered by an elastic soft shell (Figure S3J). We measured the force-displacement curve and equivalent Young's modulus of colonies with different sizes by using AFM (Figure 1C). According to the Hertzian contact theory, the indentation force F can be calculated from the indentation

depth h. Assuming that the colony is incompressible (with Poisson's ratio being 0.5), the F–h curve also depends on the Young's modulus E, the indenter radius R, and the surface tension γ. The contact region radius r is expressed as

$$r = \sqrt{Rh}.$$

Define an intrinsic material length associated with surface tension γ as

$$s = \frac{2\gamma}{E}.$$

Then the indentation force can be written as (Ding et al., 2016)

$$F = \frac{16}{9} E R^{0.5} h^{1.5} \left(1 - 0.15\frac{h}{R}\right)\left[1 + 0.88\left(\frac{s}{R}\right)^{0.87}\right].$$

Assume that the equivalent Young's modulus of the colony does not change with its size. The Young's modulus was measured from the indentation test as ~360 Pa, and the maximum surface tension in the process of colony growth is obtained approximately as $11.64\times10^{-5} N/m$.

For a semi-spherical colony, the stress inside the colony is proportional to the curvature and the surface tension in the 3D-SAC. It is reasonable to assume that the surface tension, and the induced interior stress, are proportional to the curvature and the intensity of F-actin in the colony surface layer. For the 3D colony, we define the dimensionless aspect ratio a as the ratio of the height h to the radius r_c. Then the curvature H is expressed as

$$H = \frac{4a}{(a^2+1)r_c}.$$

The differences between the internal static stress and external static stress of the colony is

$$\sigma = TH$$

The result of calculation was 3 Pa in the colony with diameter of 80 μm, and the internal pressure in the colony altered with the colony size (Figure S3K). The dynamics of the interior pressure was similar as Nanog and Oct4 expression of mESC colony, indicating a key role of force in the pluripotency maintenance. The relationship among F-actin intensity, colony geometry and Nanog and Oct4 expression was illustrated in Figure 2F.

The above theoretical result is consistent with the result based on the capillary theory. The cap-shape colony can be considered as a sessile liquid drop sitting on a substrate under the balance between the capillary force and the gravity. According to the Laplace equation, the capillary pressure P_c on the curved colony surface is calculated as $P_c - P_0 = 2\gamma H$, where P_0 is the environment static pressure outside the colony. Therefore, for the colony with diameter of 80 μm, the order of magnitude of the capillary pressure P_c is approximately 1 Pa, consistent with the value (3 Pa) estimated from the stress difference mentioned above. This pressure that maintains the 3D cap formation of the mESC colony resists the gravity $G \sim \rho g h$ of the mESC colony that breaks the cap. Based on the balance $P_c - P_0 = G$, we find that the maximum height of the colony h_{max} can hardly exceed 50 μm due to the limitation of the low surface tension.

The surface tension on the 3D-SAC surface results in the compressive pressure in the colony, which has been verified by our AFM measurement shown in Figure 1. After laser ablation on the colony surface, the release of the compressive pressure will introduce an internal flow towards the opening in the colony. This flow is governed by the low Reynolds number Stokes equation: $\nabla p = \mu \nabla^2 u$, where p and u are the pressure and the velocity respectively, and μ is the effective viscosity of the cell medium in the colony. The solution of the velocity distribution of the current situation is similar to the velocity field of a Stokes sink: $u(r) \sim 1/r^2$, where r is the distance to the opening of the laser ablation. This has been verified by the measured velocity distribution using PIV technique (Figures 2B and S3J). The phenomenon of such flow is ubiquitous with the presence of surface tension, for instance, a drainage flow from the surface of a droplet when a liquid bridge is established and breaks the droplet surface.